**Cell Reports, Volume *30***

## Supplemental Information

# A P53-Independent DNA Damage Response Suppresses Oncogenic Proliferation and Genome Instability

**Katerina D. Fagan-Solis, Dennis A. Simpson, Rashmi J. Kumar, Luciano G. Martelotto, Lisle E. Mose, Naim U. Rashid, Alice Y. Ho, Simon N. Powell, Y. Hannah Wen, Joel S. Parker, Jorge S. Reis-Filho, John H.J. Petrini, and Gaorav P. Gupta**

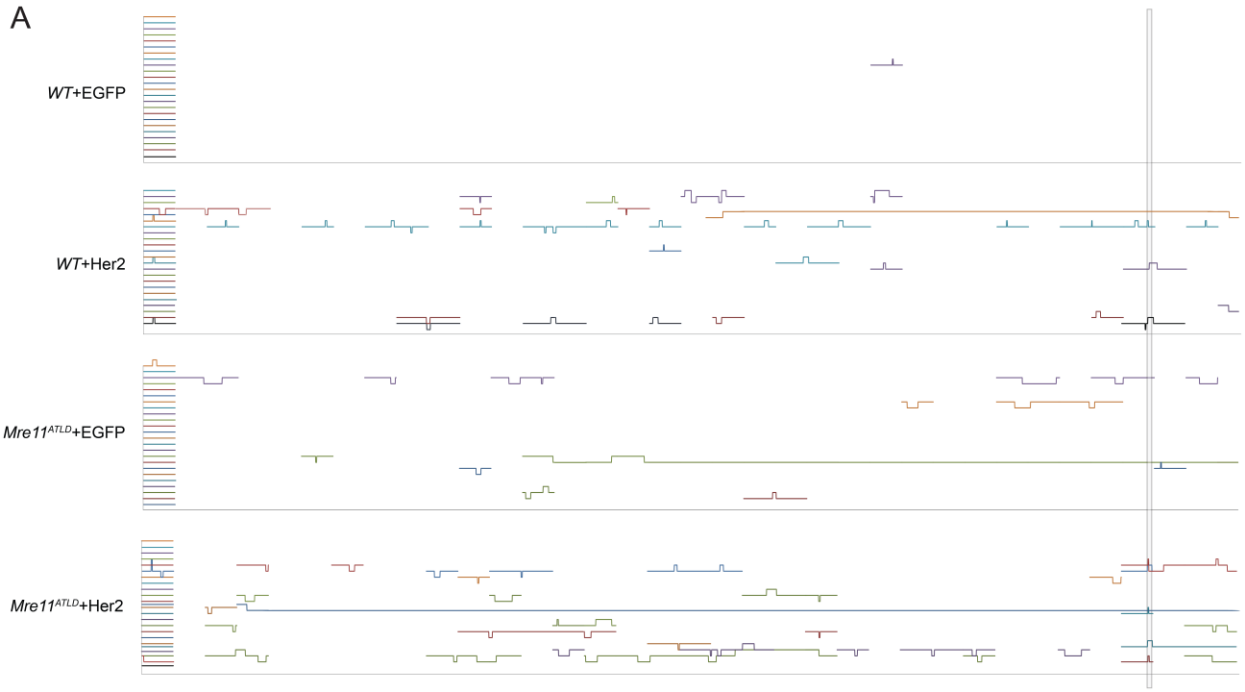


B

Number of genomic bins with copy loss

| | 0 | 1 | 2 | 3 | 4 | 5 | 6 | 7 | 8 | 9 | 10 |
|---|---|---|---|---|---|---|---|---|---|---|---|
| WT EGFP | 92706 | 35 | 0 | 0 | 0 | 0 | 0 | 0 | 0 | 0 | 0 |
| WT Her2 | 80551 | 10527 | 1431 | 163 | 37 | 2 | 30 | 0 | 0 | 0 | 0 |
| Mre11 EGFP | 68103 | 20285 | 3519 | 819 | 15 | 0 | 0 | 0 | 0 | 0 | 0 |
| Mre11 Her2 | 46261 | 35256 | 9348 | 1457 | 324 | 68 | 18 | 9 | 0 | 0 | 0 |

Number of genomic bins with copy gains

| | 0 | 1 | 2 | 3 | 4 | 5 | 6 | 7 | 8 | 9 | 10 |
|---|---|---|---|---|---|---|---|---|---|---|---|
| WT EGFP | 92368 | 312 | 27 | 25 | 9 | 0 | 0 | 0 | 0 | 0 | 0 |
| WT Her2 | 75496 | 14074 | 2467 | 608 | 41 | 46 | 0 | 1 | 8 | 0 | 0 |
| Mre11 EGFP | 83793 | 8071 | 667 | 129 | 60 | 12 | 9 | 0 | 0 | 0 | 0 |
| Mre11 Her2 | 81661 | 9306 | 1281 | 298 | 62 | 102 | 7 | 2 | 4 | 18 | 0 |

**Supplementary Figure S1: Higher resolution view of Her2-induced CNAs in Chromosome 1, Related to Figure 1.**

A) A copy number lineplot of chromosome 1 is shown to illustrate the resolution of individual CNAs detected by scWGS. The minimum aberration size visible is 100 Kb. The shaded region indicates the locus that contains the *Parp1* gene. This locus exhibits copy number gains in 4/24 *WT*+Her2 pMMECs, and 5/24 *Mre11*$^{ATLD}$+Her2 pMMECs, but not in pMMECs with either the *WT*+EGFP or *Mre11*$^{ATLD}$+EGFP genotypes. B) Summary table of genomic bins that exhibit recurrent copy number gains and losses stratified by genotype. Only 0.1% of genomic bins were recurrently gained in at least 5 cells in *Mre11*$^{ATLD}$ + Her2 pMMECs.

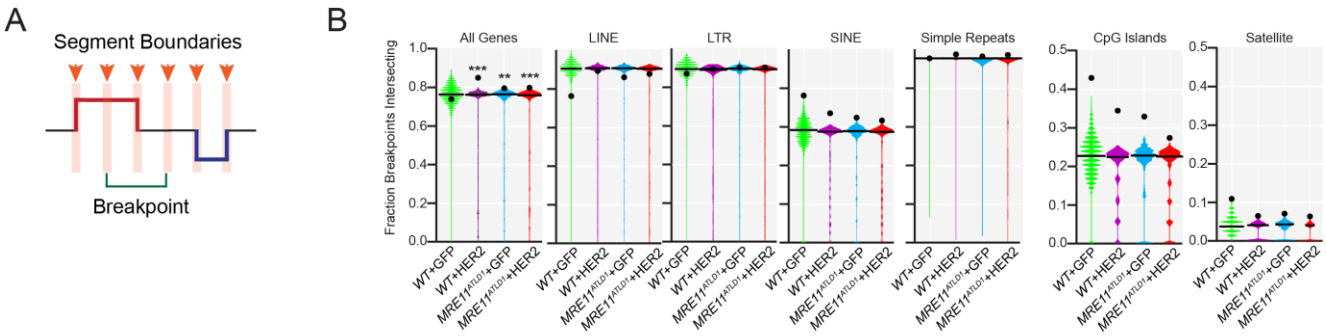


**Supplementary Figure S2: Supporting data showing aberration breakpoints are associated with genes, Related to Figure 2.**

A) Breakpoint regions are defined as the span from the start coordinate of the segment just prior to a copy number change through the stop coordinate of the first segment containing the copy number change. Thus, breakpoint regions are two segments in length or 50 Kb on average. B) Analysis of enrichment of genomic features within breakpoint regions identified in each genotype. Violin plots show the empirical null distribution of intersections based upon 10,000 shuffle permutations as described in the methods. Black line in violin plots is the median value. The black dot in each shows the observed value. Empirical p-values. * $0.03 \leq p < 0.05$; ** $0.01 \leq p < 0.03$; *** $p < 0.01$.

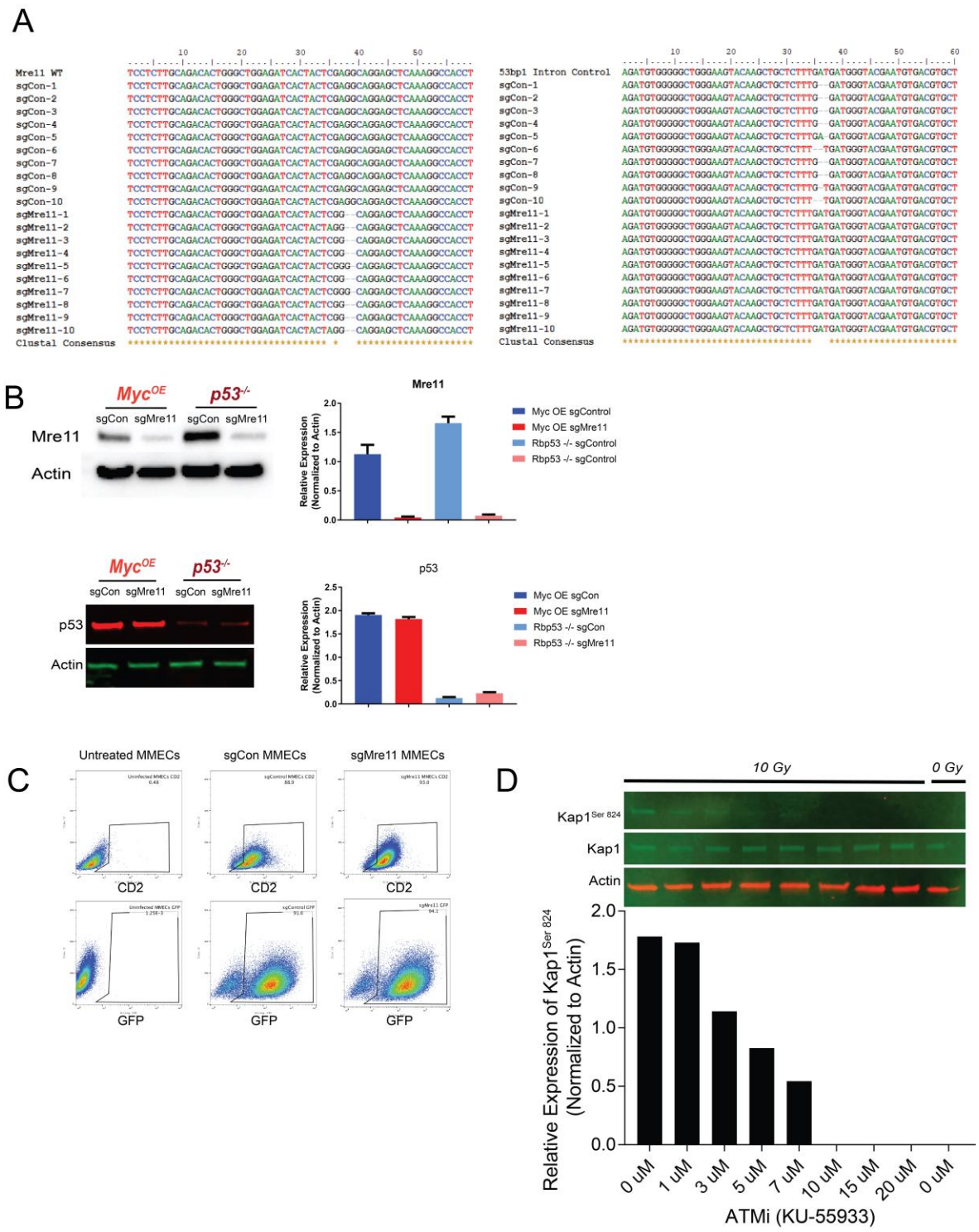


**Supplementary Figure S3: Supporting data showing Mre11 suppresses oncogenic proliferation in primary mammary epithelial cells, Related to Figure 3.** A) Validation of specificity and efficacy of target-site mutation by sgMre11 and sgControl. Shown are sequencing results of clones derived from sgRNA transduced cells used in this study showing small deletion in Mre11 as a result of sgMre11 CRISPR. Cloning and sequencing methods described in methods. B) Western blotting analysis confirming knock down of Mre11 and Trp53 in the appropriate genotypes when Cre is activated upon transduction of pMMECs with Cre-sgRNA. C) Dot plots of CD2 and GFP activations in pMMECs post Cre-sgRNA transduction to determine the efficiency of conditional transgene activation. D) Western blot confirming inhibition of ATM-mediated phosphorylation of Kap1 in *R26*$^{Cas9}$*Rb*$^{-/-}$*Trp53*$^{-/-}$ pMMECs with KU-55933 at different doses.

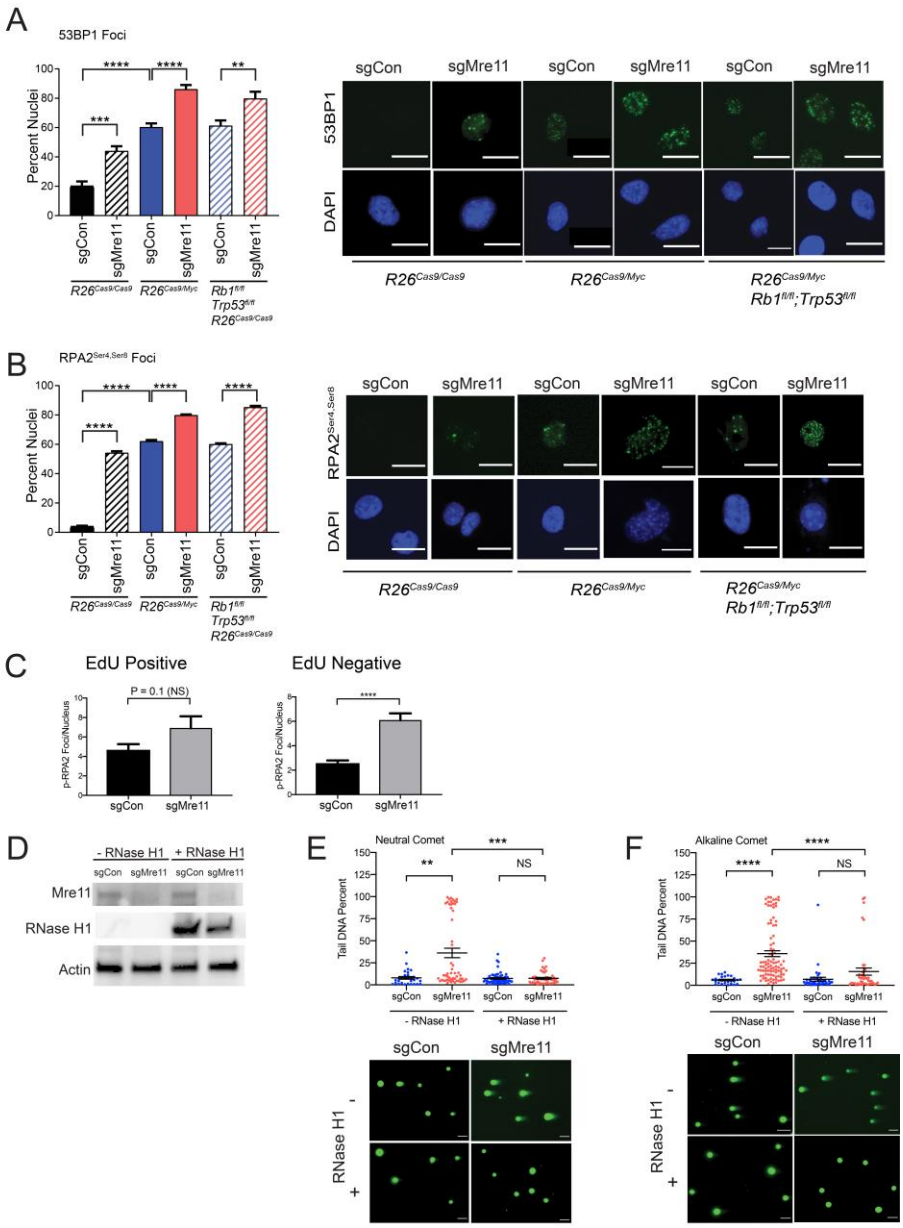


**Supplementary Figure S4: Supporting data showing Mre11 suppresses oncogene-induced DNA damage, Related to Figure 4.** A-B) Bar graph (Left) and representative images (Right) of the percent of cellular nuclei with ≥5 foci of A) 53BP1 or B) p-RPA2 in pMMECs with the indicated genotypes 3 days after transduction with Cre-sgControl versus Cre-sgMre11. C) Analysis of p-RPA2 foci per nucleus in *R26*$^{Cas9}$*Rb1*$^{fl/fl}$*Trp53*$^{fl/fl}$ pMMECs stratified by EdU staining after a 30 minute EdU pulse. D) Confirmation of Mre11 destabilization and RNase H1 expression in *R26*$^{Cas9}$*Rb1*$^{fl/fl}$*Trp53*$^{fl/fl}$ pMMECs transduced with Cre-sgControl-LumiFluor, Cre-sgMre11-LumiFluor, Cre-sgControl-RNaseH1, or Cre-sgMre11-RNaseH1, respectively. E-F) Quantification of tail DNA percentage measured by E) Neutral or F) Alkaline COMET assay in *R26*$^{Cas9}$*Rb1*$^{fl/fl}$*Trp53*$^{fl/fl}$ pMMECs transduced with the indicated sgRNA with or without RNase H1 co-expression. Representative images of the respective COMET assays are shown in the lower panels. A) – F) **, p<0.01; ***, p<0.001; ****, p<0.0001, calculated using a two-tailed Mann-Whitney test.

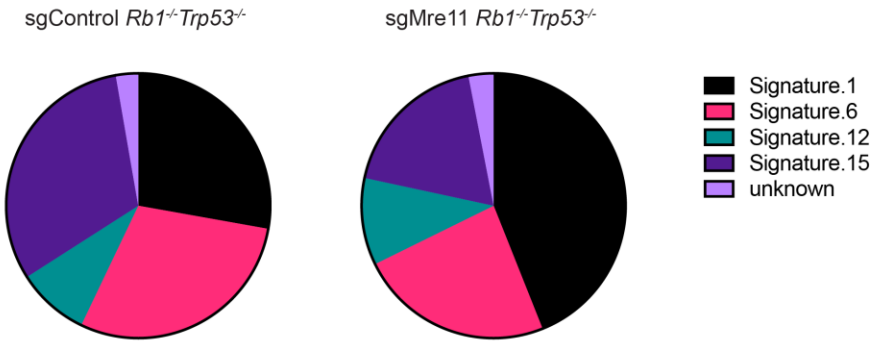


**Supplementary Figure S5: Mutation signatures are not significantly altered in control versus Mre11 hypomorphic *Rb1*$^{-/-}$*Trp53*$^{-/-}$ breast tumors, Related to Figure 5.** Relative contributions of COSMIC mutation signatures to the observed single nucleotide variations for 3 *WT* and 3 *Mre11* hypomorphic tumors was estimated using deconstructSigs. No statistically significant difference in mutation signature representation was identified.

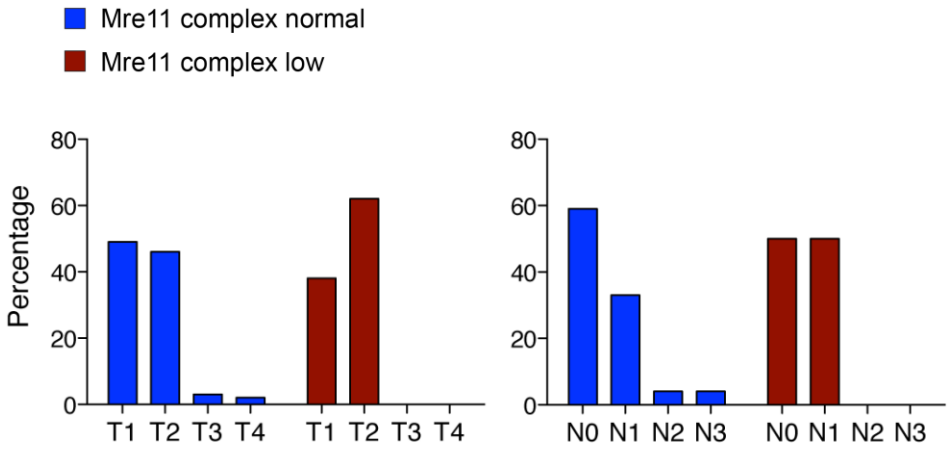


**Supplementary Figure S6: No significant differences in tumor or nodal size at initial clinical presentation based on Mre11 complex status, Related to Figure 6.** The distribution of T- and N- staging in the breast cancer cohort, stratified by Mre11 complex staining status. No significant differences in stage of disease at clinical diagnosis, despite the marked difference in clinical outcomes shown in Figure 6.